IEEE Access
Multidisciplinary | Rapid Review | Open Access Journal

Received April 22, 2020, accepted May 26, 2020, date of publication June 2, 2020, date of current version June 12, 2020.

Digital Object Identifier 10.1109/ACCESS.2020.2999515

Using Vertically Separated MIMO in Ship-to-Ship Communications

AHMED ABDELMOATY[1], (Graduate Student Member, IEEE), GHASSAN DAHMAN[1,2], (Member, IEEE), AMEN ALLAH BOUSSELMI[1], GWENAEL POITAU[1,2], (Member, IEEE), AND FRANÇOIS GAGNON[1], (Senior Member, IEEE)

[1]Resilient Machine learning Institute (ReMI) of the École de Technologie Supérieure (ÉTS), University of Quebec, Montreal, QC HC3 1K3, Canada
[2]Ultra Electronics TCS, Montreal, QC H4T 1V7, Canada

Corresponding author: Ahmed Abdelmoaty (hmed.Abdelmoaty@lacime.etsmtl.ca)

This work was supported by the NSERC-Ultra Electronics TCS Industrial Chair in High-Performance Wireless Emergency and Tactical Communications at École de Technologie Supérieure (ÉTS), University of Quebec.

ABSTRACT It is well established that the performance of communication systems is improved when deploying multiple antennas at one or both of the transmit/receive sides; and the amount of the gained improvement depends on the level of multipath richness of the propagation channel. In ship-to-ship overwater channels, quantifying such an improvement is not an easy task due to the effect of evaporation duct on imposing complex range- and height-dependent patterns of the received signal level. In this study, based on the parabolic equations (PE) method and using realistic evaporation duct distributions, we conduct extensive simulations in order to quantify the link-level improvement achieved when using 2×2 vertically-spaced Multiple-Input Multiple-Output (MIMO) systems against 1×2 Single-Input Multiple-Output (SIMO) and Single-Input Single-Output (SISO) systems. Then, we analyze the implication of such link improvement on the performance of a system comprised of a network of randomly distributed ships. When evaluating the outage throughput at the 2^{nd} percentile using realistic system parameters, it was found that 2×2 MIMO-MRC (maximum ratio combining) systems with 1 m antenna spacing are able to improve the outage throughput by three-fold compared to SISO systems. This improvement increases to one order of magnitude when the antenna spacing increases to 10 m. It was also found that, in all cases, assuming using the same vertical spacing, 1×2 SIMO-MRC systems capture about 60% of the improvement achieved by 2×2 MIMO-MRC systems. On the other hand, 1×2 SIMO-DIV (diversity combining) systems are very sensitive to antenna spacing, and when assuming using the same vertical spacing, they can capture from 20% and up to 55% of the improvement achieved by 2×2 MIMO-MRC systems if the antenna spacing increases from 1 m to 10 m, respectively.

INDEX TERMS Evaporation duct, multiple-antenna ship-to-ship communications, radio-wave overwater propagation.

I. INTRODUCTION

There is a continuous increase in demand for reliable and high throughput maritime wireless communication systems. Utilizing currently operating terrestrial systems such as WiMAX and LTE represents a cost-effective option to fulfill this need. However, the performance of communication systems in overwater environments depends heavily on the complex and unpredicted interaction between the propagation characteristics of the maritime channel and several system aspects such as the operating frequency, dynamics of the communicating nodes, antenna heights, antenna spacing, etc., [1], [2].

Multiple-Input Multiple-Output (MIMO) systems were introduced as promising successors for Single-Input Single-Output (SISO) systems. Using multiplexing gain and diversity gain, MIMO systems are known to be more efficient than SISO in terms of reliability and data rates [3]. However, the spatial-multiplexing performance improvement gained by MIMO decreases as the channel spatial

The associate editor coordinating the review of this manuscript and approving it for publication was Josue Antonio Nescolarde Selva.

richness decreases which is the case of the line-of-sight overwater communications. Moreover, in maritime communications, quantifying the advantage of using MIMO is still an open question, especially for long-range communications where a variety of factors influence the performance of the system.

Ray-tracing [4], [5] and the parabolic equations [6] are two main methods used to estimate the path loss in maritime channels. They both consider the effects of the tropospheric height-dependent refractivity profile on the characteristics of the received signal. These effects include having the signal being refracted, reflected, or trapped within the ducting layer. As the signal propagates, both methods, model the total path loss as the joint contribution of the free space path loss (FSPL) and the propagation factor (PF). The pattern of the PF is complex and it is time-, range- and height-dependent. Moreover, the pattern of the PF is the decisive factor in defining many characteristics of the propagation channel such as short/long-term signal enhancements/degradations [7]–[10] and distribution of the large scale parameters [11].

Multiple-antenna signal combining is proven to be a good mitigation for the signal degradation in overwater channels [12], [13]. Yet, its effectiveness depends on the degree of de-correlation among the combined signals. In [12] it was shown that combining signals which are well-separated in the frequency domain (few GHz) will improve the performance significantly. Similar combining gain is documented if the combined signals are well-separated in the space domain [14], [15]. The main contribution of this work is to evaluate the improvement that can be gained from using multiple-antenna systems in maritime communications, where: 1) we use realistic evaporation duct distributions, and 2) we assume realistic system parameters supporting two possible diversity combining schemes.

The rest of this paper is organized as follows. In Sections II and III, we introduce the propagation environment model and the system model, respectively. In Section IV, we detail the simulation setup. Then, in Section V, we discuss the main results. Finally, in Section VI, we state the conclusion of this work.

II. MODELING THE PROPAGATION ENVIRONMENT

A. THE EVAPORATION DUCT REFRACTIVITY PROFILE

For each simulated link, we assume line-of-sight communications to take place in the overwater propagation environment. Hence, the propagation environment is fully characterized by the height-dependent refractivity profile, where the tropospheric radio refractive index (n) is a function of the atmospheric parameters: pressure, wind, temperature, and humidity [16], [17]. Since the variation of the refractive index is very small, it is usually expressed in N units where:

$$N = 77.6\frac{P}{T} + 3.73 \times 10^5 \frac{e}{T^2} \tag{1}$$

where e is the water vapor pressure (mbar), T is the temperature (°K), and P is the pressure (mbar).

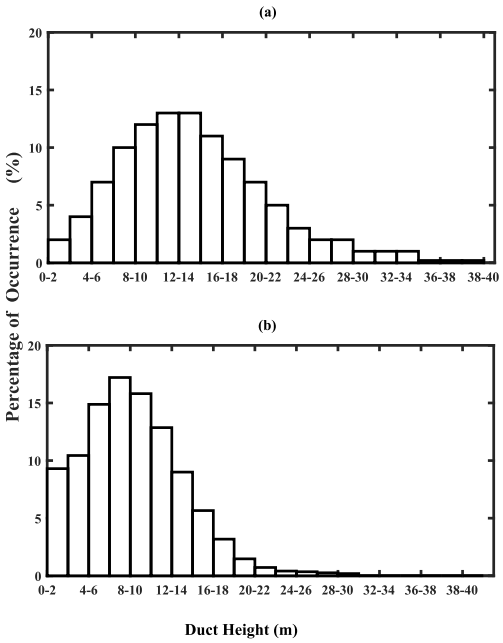

FIGURE 1. The relative frequency histograms of the duct height in two regions. (a) The Aegean Sea [7], (b) The English Channel [12].

To account for the earth surface curvature, the modified refractive index M was introduced as [16, Sec. 3.7]:

$$M = N + \frac{z}{a} \times 10^6 = N + 157z \tag{2}$$

where z is the height in km above the earth's surface, a is the Earth's radius (i.e., $a = 6,378$ km).

The modified refractivity profiles of evaporation ducts can be modeled with a height-dependent logarithmic function which changes with the duct height as [18]:

$$M(z) = M_0 + 0.13z - 0.13\delta \ln\left(\frac{z + z_0}{z_0}\right) \tag{3}$$

where M_0 is the value of the modified refractivity at the surface which is taken as 300 M-units, z is the vertical height in m, z_0 is the aerodynamic roughness which is assumed as 1.5×10^{-4} m, δ is the duct height in m, which signifies the height at which $M(z)$ reaches its minimum value [18].

B. DISTRIBUTIONS OF THE EVAPORATION DUCT HEIGHT OF TWO METEOROLOGICAL REGIONS

Since the overwater propagation environment is characterized by the duct height, it is important to adopt a realistic duct distribution for our simulations. In this regard, we use two different distributions for the duct height representing areas with distinct meteorological characteristics. Figure 1 shows the relative frequency histograms of the duct height in the Aegean sea and the English Channel [7], [12]. It is self-explanatory that these two regions have different duct height distributions, where the higher the temperature, the more the chances of encountering a higher duct.

III. SYSTEM MODEL

A. ANTENNA CONFIGURATIONS AND DIVERSITY COMBINING SCHEMES

In this study, we evaluate the received signal strength using the parabolic equation software tool (PETOOL), which is a free and online-available Matlab-based one-way/two-way split step parabolic equation software that was developed for the analysis and visualization of radio-wave propagation over variable terrain and through the homogeneous and inhomogeneous atmosphere [6]. The PETOOL supports different ducting profiles as well as range-dependent ducting profiles; however, all results reported in this work are for overwater range-independent evaporation duct M-profiles.

The simulations took place for a maximum range of 100 km in steps of 10 m. The inputs to the simulations are: 1) the evaporation duct profile characterizing the propagation environment, with duct height changes from 1 to 40 m, 2) the operating frequency (three different frequencies are simulated 1, 2, and 4 GHz), and 3) the antenna parameters (beam pattern, direction, and polarization). Based on that, the PETOOL estimate the range- and height-dependent PF which is used to realize the total path loss as [6]:

$$PL(dB) = FSPL(dB) - PF(dB) \tag{4}$$

where PL is the resulting total path loss, $FSPL$ is the free-space path loss and PF is the propagation factor.

We assume each communication node (i.e., ship) to be provided with one or two antenna elements, where we simulate the following cases: SISO, 1×2 SIMO, and 2×2 MIMO. We assume the inter-element vertical spacing to vary between 1 and 10 m.

Besides the reference SISO case, three diversity combining schemes are studied: 1) SIMO-DIV (selection diversity combining): the strongest received signal is selected for detection [19], 2) SIMO-MRC (maximum ratio combining): the received signals are co-phased and phase-coherently added [19], and 3) MIMO-MRC: the beamforming vector is chosen to be the eigenvector corresponding to the maximum eigenvalue λ_{max} of $H^{\dagger}H$, where H is the 2×2 MIMO channel and $(.)^{\dagger}$ is the Hermitian conjugate operator, for more details on the way of applying the beamforming vector of MIMO-MRC we refer the readers to [20].

B. MIMO CHANNEL MODEL

The output of the PETOOL is the PL of a SISO system, which is a scalar quantity. Since the evaluated combining schemes are operated on complex quantities representing the channel realizations, we perform the simulations based on the PETOOL outputs as follows. First, for each SISO case i.e., specific duct height, specific transmit and receive antenna heights, we simulate the SISO channel gain using (4). Then, we impose a random phase $x \sim U(0, 2\pi)$ on each SISO channel gain. Finally, based on the resulting complex SISO gains, the corresponding SIMO, or MIMO channels are realized and the corresponding SIMO-DIV, SIMO-MRC, and MIMO-MRC gains are calculated.

By definition, since we evaluate the performance based on instantaneous realizations of the channel which are assumed to be known at the transmitter/receiver, the distribution of the imposed phase x doesn't affect the performance of the SISO, SIMO-DIV, nor SIMO-MRC combining schemes. On the other hand, the distribution of x surly affects the performance of the MIMO-MRC combiner scheme. It is well known that the more the de-correlation (among the MIMO channel entries) introduced by the imposed phase, the better the performance of spatial multiplexing MIMO schemes. Consequently, it can be concluded that imposing a phase with the maximum possible randomness i.e., $x \sim U(0, 2\pi)$ would result in optimistic performance evaluation for spatial multiplexing MIMO schemes. However, since in this work we are interested in evaluating the performance of the MIMO-MRC scheme, we will show in the sequel that assuming the maximum possible randomness associated with the imposed phase i.e., $x \sim U(0, 2\pi)$, results in a very conservative performance of the MIMO-MRC system.

In MIMO-MRC, the beamforming vector is chosen to be the eigenvector corresponding to the maximum eigenvalue λ_{max} of $H^{\dagger}H$, where $(.)^{\dagger}$ is the Hermitian conjugate operator [20]. Using Singular-Value Decomposition (SVD), and given that H is a 2×2 matrix, then we can write:

$$\begin{aligned} H^{\dagger}H &= V\Sigma^{\dagger}U^{\dagger}U\Sigma V^{\dagger} = V(\Sigma^{\dagger}\Sigma)V^{\dagger}, \\ &= \sigma_1^2 v_1 v_1^{\dagger} + \sigma_2^2 v_2 v_2^{\dagger}, \\ &= \lambda_{max} v_1 v_1^{\dagger} + \lambda_{min} v_2 v_2^{\dagger}, \end{aligned} \tag{5}$$

where $U = [u_1, u_2]$ and $V = [v_1, v_2]$ are unitary matrices. Σ is a square diagonal matrix with elements σ equal to the singular values of $H^{\dagger}H$ such that $\sigma_1 \geq \sigma_2$, $\lambda_{max} = \sigma_1^2$ and $\lambda_{min} = \sigma_2^2$.

Hence, the MIMO-MRC beamforming vector is associated with the rank-1 approximation of $H^{\dagger}H$ [22, Sec. 7.1], which means that, for a specific channel matrix realization, the lowest MIMO-MRC performance will take place when the imposed phase introduces the maximum possible randomness i.e., $x \sim U(0, 2\pi)$. Figure 2 demonstrates this result where we plot the empirical cumulative distribution function (ECDF) of the ratio $10\log_{10}(\frac{\lambda_{max}}{\lambda_{max}+\lambda_{min}})$ resulting from applying the MIMO-MRC combiner to a specific channel realization after imposing phases with different distributions. The plots show clearly that the adopted phase distribution i.e., $x \sim U(0, 2\pi)$ is associated with the smallest performance for MIMO-MRC. By definition, $0 \leq \lambda_{min} \leq \lambda_{max}$, hence, the degradation effect of the phase distribution i.e., $x \sim U(0, 2\pi)$ on the MIMO-MRC performance is between 0 and -3 dB.

C. CHANNEL GAIN AND ACHIEVED THROUGHPUT FOR THE DIFFERENT COMBINING SCHEMES

For each considered scheme, the achieved throughput at an average signal-to-noise ratio (SNR) is calculated as:

$$R = B\log_2(1 + SNR_k) \quad \text{bps}, \tag{6}$$

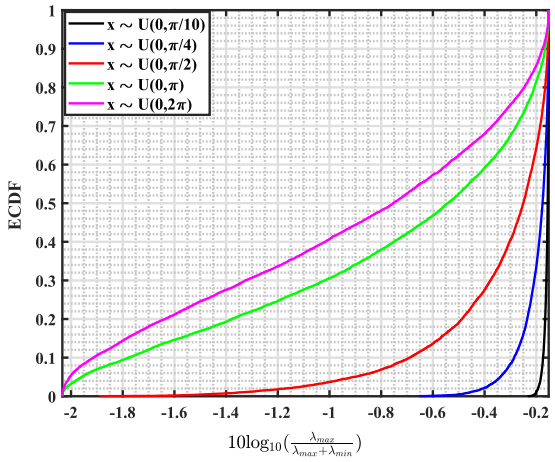

FIGURE 2. The effect of the distribution of the imposed phase x on the performance of the MIMO-MRC combining scheme.

where B is the bandwidth and the subscript k in SNR_k signifies the considered antenna configuration and combining schemes which can be one of the four possibilities: SISO, SIMO-DIV, SIMO-MRC, and MIMO-MRC.

The resulting channel gain and the throughput may be considered to be a random variable. Therefore, the link quality —i.e. the channel gain, G (dB), and the achieved throughput, R (Mbps)— are evaluated in terms of their outage at probability p, which are defined through the relationship:

$$\text{Prob}[G \leq G_{k,out}] = p \tag{7}$$

$$\text{Prob}[R \leq R_{k,out}] = p \tag{8}$$

where the subscript k signifies the considered antenna configuration and combining schemes; $G_{k,out}$ and $R_{k,out}$ are the outage channel gain and the outage throughput, respectively (both evaluated at the pth percentile).

IV. SIMULATION SETUP

In our analysis, we assume communications to take place between two ships. On one side, we assume a big ship where the height of the top antenna is fixed at 40 m above the sea level. On the other side of the link, we assume the possibility of having different ship sizes where we assume the top antenna to vary between 40 to 15 m. On both sides of the link, we consider the vertical antenna spacing to vary between 1 to 10 m and in the case of MIMO, we assume similar vertical antenna spacing at both ends. To be able to study the improvement achieved when using multiple antennas for a link with specific parameters (i.e., specific: operating frequency, duct height, antenna spacing, and combining technique), we average out the effect of the antenna height as follows. First, for each specific antenna height, the instances of the metric quantifying the link, e.g., G or R, are collected and the resulting empirical cumulative distribution function (ECDF) is assessed at a specific percentile p based on (7) and (8) to find the corresponding outage gains ($G_{k,out}$) or outage throughputs ($R_{k,out}$). Then, all calculated values of $G_{k,out}$ or $R_{k,out}$ for all possible antenna heights

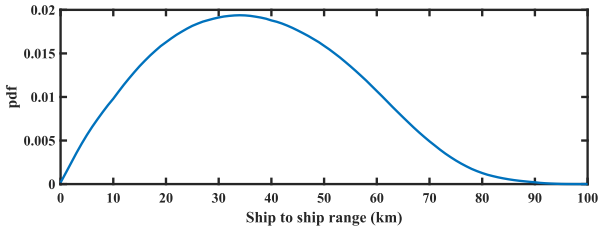

FIGURE 3. The distribution of the link range of the simulated ship-to-ship scenario.

are averaged. The resulting outage gain and outage throughput characterize the quality of the link corresponding to its specific operating frequency, duct height, antenna spacing, and combining technique, assuming an equal probability of all considered antenna heights. For all reported results in the sequel, the outage gain or outage throughput will be evaluated at the 2nd percentile.

Moreover, in order to perform the evaluation using realistic link range, we assume the existence of 10 communication nodes (i.e., ships) that are randomly distributed according to a Poisson Point Process (PPP) in a square simulation area with a side length of 70 km. Figure 3 represents the resulting range distribution among the ships, which has a median value of about 37 km.

Using the propagation factor obtained from the PETOOL, the channel gain is computed, then the signal-to-noise ratio (SNR) for each system i.e., MIMO-MRC, SIMO-DIV, SIMO-MRC, SISO is computed using [21]:

$$SNR_k(dB) = P_t + G_t + G_r + G_k - PL - L_s - F_n - B - N_0 \tag{9}$$

where P_t is the transmitted power (dBm). G_t, and G_r are the antenna gains (dB) at the transmitter and receiver, respectively. G_k (dB) is the gain associated with the k^{th} antenna combining scheme. PL (dB) is the path loss. L_s (dB) is the system loss accounting for connectors, cable losses, etc. F_n (dB) is the receiver noise figure. B (Hz) is the signal bandwidth. N_0 (dBm/Hz) is the noise power density. Then, using $snr = 10^{\frac{1}{10}SNR_k}$, the achieved throughput of each system is computed as given in (6). In our simulations, we assume $P_t = 30$ dBm, $G_t = G_r = 8$ dB, $L_s = 1$ dB, $F_n = 10$ dB, $B = 20$ MHz, $N_0 = -174$ dBm.

Extensive Monte Carlo simulations are conducted in order to evaluate the performance of the SISO, SIMO-DIV, SIMO-MRC, and MIMO-MRC systems at different frequencies, duct heights, and antenna spacing. For each considered case, 5000 different realizations of the network topology (i.e., distributions of the ships) are simulated. Moreover, for each network topology, 10 realizations of the multiple-antenna channels are generated (by imposing a random phase).

V. RESULTS AND DISCUSSIONS

Figure 4 depicts $G_{k,out}$ versus the range. In this plot, a 10 m antenna spacing is considered. This figure shows $G_{k,out}$ for the four considered systems (SISO, SIMO-DIV, SIMO-MRC

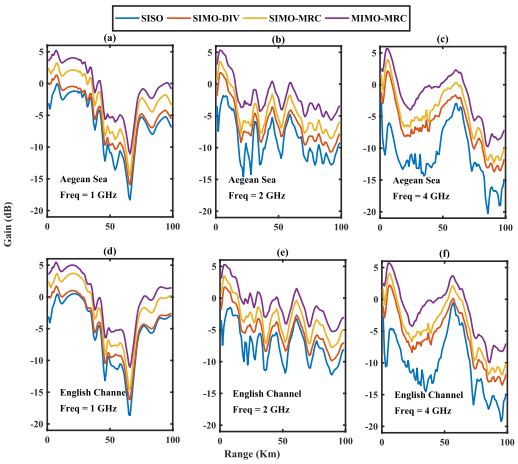

FIGURE 4. The 2^{nd} percentile of the antenna combining gain versus range for the different multiple-antenna systems at 10 m antenna spacing. Two duct distributions: the Aegean Sea (1^{st} row) and the English Channel (2^{nd} row). Operating frequencies: 1, 2, and 4 GHz.

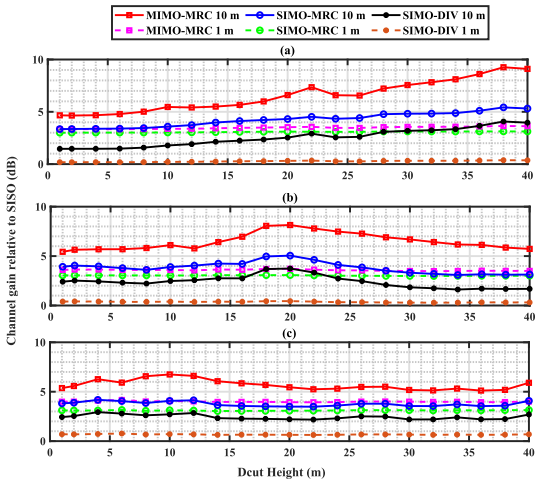

FIGURE 5. The channel gain improvement relative to SISO (evaluated at the 2^{nd} percentile) for different duct heights, for the English Channel, at frequencies: (a) 1 GHz, (b) 2 GHz (c) 4 GHz.

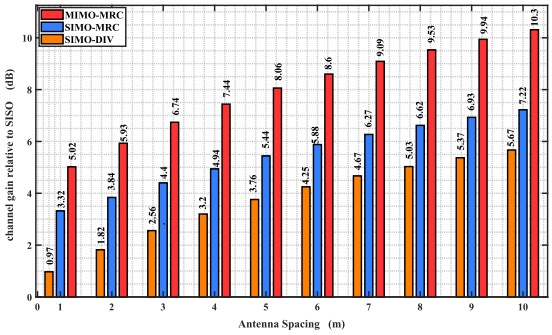

FIGURE 6. The channel gain improvement relative to SISO (evaluated at the 2^{nd} percentile) for antenna spacing 1 m to 10 m at 2 GHz for the English Channel.

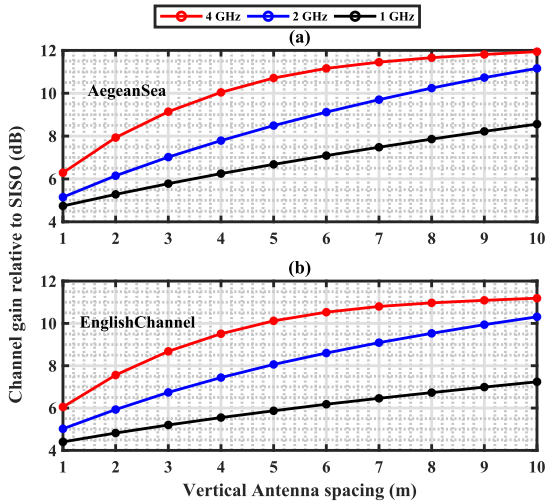

FIGURE 7. The channel gain improvement of MIMO-MRC relative to SISO (evaluated at the 2^{nd} percentile). Antenna spacing varies from 1 m to 10 m at 2 GHz. (a) Aegean Sea, (b) English Channel.

& MIMO-MRC), for the Aegean Sea and the English Channel duct distributions, and operating frequencies 1, 2, and 4 GHz. From this figure, we can clearly identify the strong impact of the range on the behavior of all antenna combining schemes. However, it is also evident that the duct distributions of the two meteorological areas have an insignificant effect on the reported performance criterion (i.e., the 2^{nd} percentile) for the different schemes. Similarly, we can see that as the operating frequency increases, the contribution of using multiple-antenna systems on improving the quality of the links becomes more remarkable. These observations will be analyzed in-depth in the remaining sections. We will also evaluate the improvement in the antenna combining gain, $G_{k,out}$, and the throughput, $R_{k,out}$, that can be achieved by the different antenna combining schemes relative to SISO.

A. GAIN IMPROVEMENT OF THE DIFFERENT COMBINING SCHEMES

Figure 5 shows the channel gain improvement achieved by SIMO-DIV, SIMO-MRC, and MIMO-MRC, relative to SISO, with antenna spacing of 1 and 10 m, as the duct height increases from 1 to 40 m for operating frequencies 1 GHz, 2 GHz, and 4 GHz. When the duct height increases, only at the 1 GHz frequency, the improvement of relative channel gains for all combining schemes (almost) monotonically increases. For example, at 1 GHz with 10 m antenna spacing, the SIMO-DIV, SIMO-MRC & MIMO-MRC increases from 1 dB, 3 dB & 5 dB, at 1 m duct height to 4 dB, 5.5 dB & 9 dB at 40 m duct height, respectively. However, at frequencies 2 and 4 GHz, we see that this monotonic trend disappears. This change in behavior at the different operating frequencies will be explained based on the space-correlation function of the PF in section V-C.

Figure 6 shows the channel gain of SIMO-DIV, SIMO-MRC, and MIMO-MRC relative to SISO at 2 GHz for the English Channel. It can be seen that as the antenna spacing increases from 1 to 10 m, MIMO-MRC records between 4 to 5 dB more gain compared to SIMO-DIV, 1.5 to 3 dB gain compared to SIMO-MRC. In general, we can conclude the following two points: 1) SIMO-MRC achieves more than

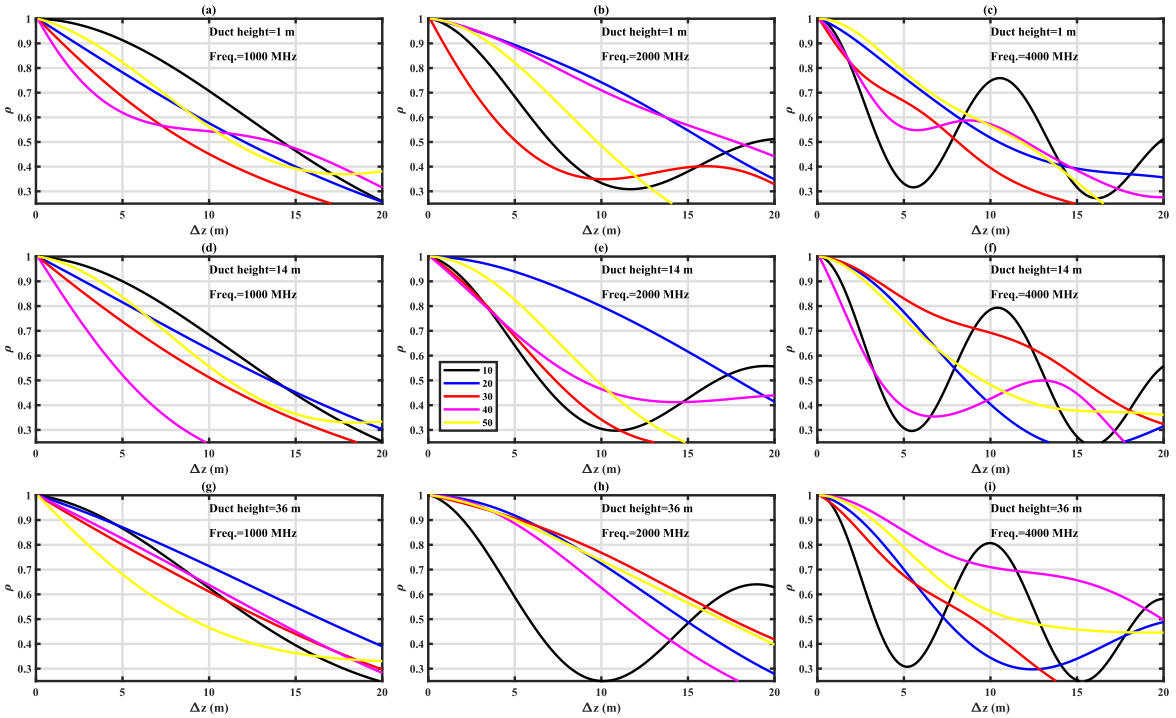

FIGURE 8. The space-correlation function of the propagation factor at different operating frequencies (1, 2, & 4 GHz), different duct heights (1, 14, & 36 m) and at different ranges (10, 20, 30, 40, & 50 km).

60% of the gain obtained by MIMO-MRC for all considered antenna spacings, and 2) the gain improvement achieved by SIMO-DIV is sensitive to the amount of antenna spacing, for example, at 1 m spacing, SIMO-DIV achieves only 20% of what MIMO-MRC records; however, this gain jumps to about 55% when the antenna spacing is 10 m.

B. EFFECT OF VERTICAL ANTENNA SPACING AT DIFFERENT FREQUENCY BANDS

Figure 7 presents the channel gain improvement realized with MIMO-MRC relative to SISO with vertical antenna spacing varies from 1 to 10 m. We assume three different frequency bands: 1, 2, and 4 GHz, and the two duct distributions of figure 1. From figure 7, we can deduce the following:

- Comparing the two considered regions (i.e., the Aegean Sea and the English Channel), there is no significant difference in terms of the gain that can be achieved when using MIMO-MRC. For example, in both environments, using MIMO-MRC with 1 m vertical spacing improves the channel gain by 4 to 6 dB. This finding indicates that even with such small antenna spacing and regardless of the operating frequency, not less than 4 dB of gain is achieved when using MIMO-MRC.
- The larger the antenna spacing, the less the deep fading occurrences, which has a significant effect on improving the link reliability. This improvement can reach up to 12 dB gain when the antenna spacing is 10 m.
- Depending on the operating frequency, the achieved gain as the antenna spacing increases might exhibit a saturation behavior i.e., an antenna spacing beyond which there is no considerable gain can be realized. For example, based on figure 7, at 1 GHz, the amount of the gain improvement (reported per 1 m increase in antenna spacing) of the MIMO-MRC decreases from 0.55 dB/m to 0.30 dB/m as the antenna spacing increases from 1 to 10 m. However, at 4 GHz, the gain improvement of the MIMO-MRC system diminishes faster where it decreases from 1.60 dB/m to 0.12 dB/m as the antenna spacing increases from 1 to 10 m.

When interpreting the results of figure 7, we have to consider that the reported values are the channel gain achieved relative to SISO. Therefore, when evaluating the overall link quality at different frequencies, these results should be interpreted jointly with the SISO channel gains.

C. ANALYSIS BASED ON THE SPACE-CORRELATION FUNCTION OF THE PROPAGATION FACTOR

In an effort to understand the effect of the operating frequency and vertical spacing on the channel gain improvements reported in sections V-A and V-B, we investigate the space-correlation function of the PF. Figure 8 depicts the space-correlation function of the propagation factor at different operating frequencies (1, 2, & 4 GHz), different duct heights (1, 14, & 36 m) and at different ranges (10, 20, 30, 40, & 50 km). Let's define the decorrelation distance as the antenna spacing at which the correlation of the PF drops to 0.5. From figure 8, we can observe that at 1 GHz, the decorrelation distance reaches about 20 m, which means that we will continue observing antenna combining gain even if we increase the antenna spacing beyond 10 m.

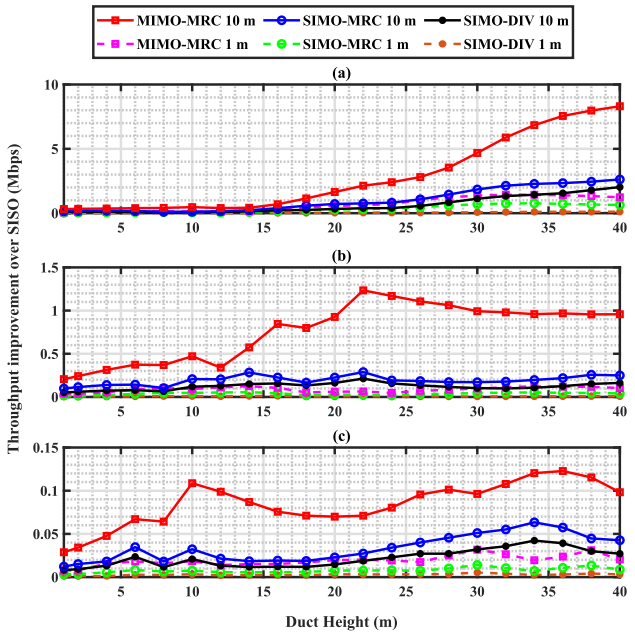

FIGURE 9. The absolute achieved throughput improvement (Mbps) compared to SISO (evaluated at the 2^{nd} percentile) st different antenna spacing and frequencies. (a) 1 GHz, (b) 2 GHz, and (c) 4 GHz.

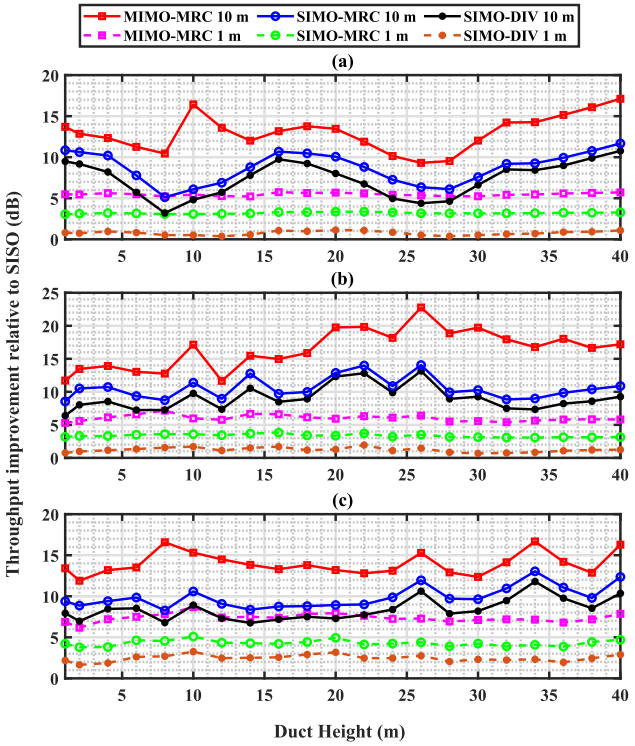

FIGURE 10. The relative achieved throughput improvement (dB) relative to SISO (evaluated at the 2^{nd} percentile) at different antenna spacing and frequencies. (a) 1 GHz, (b) 2 GHz (c) 4 GHz.

This explains the linear gain improvement with antenna spacing in figure 7. On the other hand, as the operating frequency increases, e.g., 4 GHz, the decorrelation distance decreases. Therefore, after certain antenna spacing (of a few meters), the antenna combining gain reaches a saturation level. It is also evident from figure 8 that, as the range, the duct height, and the operating frequency changes, the space-correlation function behaves in a more and more unheralded way.

D. THROUGHPUT IMPROVEMENT OF THE DIFFERENT COMBINING SCHEMES

We investigate the throughput achieved by the different antenna combining schemes under different evaporation duct heights at different operating frequencies. In all cases, we use the simulation parameters detailed in section IV.

In figure 9, we define the *absolute* throughput improvement as the amount of extra throughput (Mbps) achieved by the different multiple-antenna systems compared to the SISO system. The achieved absolute throughput improvement is plotted as duct height varies from 1 to 40 m with frequencies 1, 2, 4 GHz at two antenna spacing: 1 and 10 m. For the case of 1 GHz and 10 m spacing, the absolute throughput improvement achieved by the MIMO-MRC system increases from 0.5 Mbps at 1 m to 8 Mbps at 40 m duct height. Whereas, the absolute throughput improvement achieved by the SIMO-MRC system increases from 0.3 Mbps to 3 Mbps for the same duct height increment. Yet, the absolute throughput improvement achieved by the SIMO-DIV system is very small: goes from 0.1 Mbps at 1 m to almost 2 Mbps at 40 m duct height. For the higher frequencies i.e., 2 and 4 GHz, the achieved absolute throughput improvements by the different multiple-antenna systems persist. Nevertheless, due to the higher path loss associated with higher frequencies, these improvements are smaller compared to the 1 GHz frequency.

In figure 10, we define the *relative* throughput improvement as the ratio (expressed in dB) between the throughput achieved by the different multiple-antenna systems and the throughput achieved by the SISO system. Considering the outage throughput at the 2^{nd} percentile, with antenna spacing as small as 1 m, it can be seen that the SIMO-DIV, SIMO-MRC and MIMO-MRC achieve around 1 dB (≈125%), 3 dB (≈200%), and 5 dB (≈320%) throughput compared to SISO. When the antenna spacing increases to 10 m, this *relative* throughput improvement reaches (on average) 7 dB, 8 dB, and 13 dB for the SIMO-DIV, SIMO-MRC, and MIMO-MRC systems, respectively.

VI. CONCLUSION

In this paper, based on extensive Monte Carlo simulations, we studied the improvements that can be achieved using multiple-antenna systems in overwater communication channels. First, using the parabolic equations model for the overwater propagation channel, we analyzed the link quality for different antenna spacing, heights of evaporation duct, and operating frequencies. Second, we quantified the effect of using different multiple-antenna combining schemes on the quality of the link and, consequently, the throughput of a system comprises of randomly distributed communication nodes. It was found that using a 2×2 MIMO-MRC system with antenna spacing as small as 1 m results in improving the channel gain by 4 to 6 dB compared to SISO.

This improvement can go up to 12 dB has the antenna spacing increases to 10 m. Moreover, it was found that, in all cases, 1×2 SIMO-MRC systems are able to attain about 60% of the improvement achieved by 2×2 MIMO-MRC systems. This multiple-antenna combining gain results in significant system throughput improvement, for example, a 2×2 MIMO-MRC system demonstrates one order of magnitude outage throughput improvement (evaluated at the 2^{nd} percentile) when compared to SISO.

REFERENCES

[1] L. Y. Hui, F. Dong, and Y. S. Meng, "Near sea-surface mobile radiowave propagation at 5 GHz: Measurements and modeling," *Radioengineering*, vol. 23, no. 3, pp. 824–830, 2014.
[2] H. V. Hitney, J. H. Richter, R. A. Pappert, K. D. Anderson, and G. B. Baumgartner, "Tropospheric radio propagation assessment," *Proc. IEEE*, vol. 73, no. 2, pp. 265–283, Feb. 1985.
[3] M. Wagner, S. Nannuru, and P. Gerstoft, "Compressive MIMO beamforming of data collected in a refractive environment," *Radio Sci.*, vol. 52, no. 12, pp. 1458–1471, Dec. 2017.
[4] C. Hattan, "A ray trace model for propagation loss," Naval Command Control Ocean Surveill. Center RDT E Division, San Diego, CA, USA, Tech. Rep. 1576, 1993.
[5] G. Dahman, F. Gagnon, and G. Poitau, "Ship-to-ship beyond line-of-sight communications: A comparison between ray tracing simulations and the PETOOL," in *Proc. 32nd Gen. Assem. Scientific Symp. Int. Union Radio Sci. (URSI GASS)*, Aug. 2017, pp. 1–4.
[6] O. Ozgun, G. Apaydin, M. Kuzuoglu, and L. Sevgi, "PETOOL: MATLAB-based one-way and two-way split-step parabolic equation tool for radiowave propagation over variable terrain," *Comput. Phys. Commun.*, vol. 182, no. 12, pp. 2638–2654, Dec. 2011.
[7] S. D. Gunashekar, E. M. Warrington, and D. R. Siddle, "Long-term statistics related to evaporation duct propagation of 2 GHz radio waves in the English Channel," *Radio Sci.*, vol. 45, no. 6, pp. 1–14, 2010.
[8] S. D. Gunashekar, E. M. Warrington, D. R. Siddle, and P. Valtr, "Signal strength variations at 2 GHz for three sea paths in the British Channel Islands: Detailed discussion and propagation modeling," *Radio Sci.*, vol. 42, no. 4, pp. 1–13, Aug. 2007.
[9] D. R. Siddle, E. M. Warrington, and S. D. Gunashekar, "Signal strength variations at 2 GHz for three sea paths in the British Channel Islands: Observations and statistical analysis," *Radio Sci.*, vol. 42, no. 4, pp. 1–15, Aug. 2007.
[10] D. Couillard, G. Dahman, M.-E. GrandMaison, G. Poitau, and F. Gagnon, "Robust broadband maritime communications: Theoretical and experimental validation," *Radio Sci.*, vol. 53, no. 6, pp. 749–760, Jun. 2018.
[11] E. Dinc and O. B. Akan, "Channel model for the surface ducts: Large-scale path-loss, delay spread, and AOA," *IEEE Trans. Antennas Propag.*, vol. 63, no. 6, pp. 2728–2738, Jun. 2015.
[12] H. V. Hitney and L. R. Hitney, "Frequency diversity effects of evaporation duct propagation," *IEEE Trans. Antennas Propag.*, vol. 38, no. 10, pp. 1694–1700, Oct. 1990.
[13] S.-H. Lin, "Statistical behavior of deep fades of diversity signals," *IEEE Trans. Commun.*, vol. 20, no. 6, pp. 1100–1107, Dec. 1972.
[14] A. Vigants, "Space-diversity performance as a function of antenna separation," *IEEE Trans. Commun.*, vol. TCOMM-16, no. 6, pp. 831–836, Dec. 1968.
[15] H. Makino and K. Morita, "Design of space diversity receiving and transmitting systems for Line-of-Sight microwave links," *IEEE Trans. Commun. Technol.*, vol. TCOM-15, no. 4, pp. 603–614, Aug. 1967.
[16] G. Apaydin and L. Sevgi, *Radio Wave Propagation and Parabolic Equation Modeling*. Hoboken, NJ, USA: Wiley, 2017.
[17] A. Kukushkin, *Radio Wave Propagation in the Marine Boundary Layer*. Hoboken, NJ, USA: Wiley, 2006.
[18] I. Sirkova and M. Mikhalev, "Parabolic wave equation method applied to the tropospheric ducting propagation problem: A survey," *Electromagnetics*, vol. 26, no. 2, pp. 155–173, Feb. 2006.
[19] Y.-W. P. Hong, W.-J. Huang, and C.-C. J. Kuo, "Review of wireless communications and MIMO techniques," in *Cooperative Communications and Networking: Technologies and System Design*. New York, NY, USA: Springer, 2010, ch. 1, pp. 15–65.
[20] S. Jin, M. R. McKay, X. Gao, and I. B. Collings, "Asymptotic SER and outage probability of MIMO MRC in correlated fading," *IEEE Signal Process. Lett.*, vol. 14, no. 1, pp. 9–12, Jan. 2007.
[21] F. Gagnon, G. Dahman, and G. Poitau, "Tactical backhaul range extension using MIMO: Investigation based on ITU-R P.530," in *Proc. IEEE Can. Conf. Electr. Comput. Eng. (CCECE)*, May 2019, pp. 1–6.
[22] D. Tse and P. Viswanath, *Fundamentals of Wireless Communication*. Cambridge, U.K.: Cambridge Univ. Press, 2005.

AHMED ABDELMOATY (Graduate Student Member, IEEE) received the B.S. degree in electronics and telecommunications engineering from Al-Azhar University, Cairo, Egypt, in 2004, and the M.S. degree in electrical engineering from the King Fahd University of Petroleum and Minerals (KFUPM), Saudi Arabia, in 2017. He is currently pursuing the Ph.D. degree in electrical engineering with the École de Technologie Supérieure, University of Quebec, Canada. Since 2018, he has been with the Electrical Engineering Department, Al-Azhar University, as Lecturer Assistant. His research interests include wireless communications, communication networks, machine learning, and RF propagation.

GHASSAN DAHMAN (Member, IEEE) received the Ph.D. degree from Carleton University, Ottawa, ON, Canada, in 2010. From 2010 to 2012, he was an Assistant Professor with Umm Al-Qura University, Mecca, Saudi Arabia. He held research positions with Lund University, Lund, Sweden, from 2012 to 2016, and with the NSERC-Ultra Electronics TCS Industrial Chair, École de Technologie Supérieure (ÉTS), Montreal, QC, Canada, from 2016 to 2018. He is currently with ULTRA-TCS, Montreal, QC, Canada. His main research interests are radio propagation and channel modeling, including massive multiple-input multiple-output (MIMO) systems, distributed antenna systems, overwater point-to-point communications, and anomalous propagation of microwaves in the troposphere.

AMEN ALLAH BOUSSELMI received the bachelor's degree in electronics and telecommunications engineering from the National School of Electronics and Telecommunications of Sfax (ENETCOM), and the M.Eng. degree in electrical engineering from the École de Technologie Supérieure (ÉTS), University of Quebec, Canada, in 2018. He is currently a Research Professional with ReMI (Resilent of critical communication). His research interests include wireless communications, reinforcement learning, and RF propagation.

GWENAEL POITAU (Member, IEEE) received the bachelor's, master's, and Ph.D. degrees in physics and electrical engineering from Telecom Saint-Etienne and INSA Lyon, France. He has more than 18 years of experience developing wireless communication systems for the telecom and defense markets. He began his career with Wavesat in Montreal developing signal processing algorithms and ASIC architectures for 4G chipsets. He was then promoted as the Technical Lead for LTE development. He continued to work on LTE at Interdigital, where he generated Intellectual Property on Device-to-Device communications and participated to LTE Rel. 12 standardization. In July 2010, he joined Ultra Electronics TCS, as Wireless Architect for the new ORION radio product line and was promoted the Chief Technology Officer, in September 2013. In addition to its CTO role, he took the Head of Engineering position, in 2016. In 2019, he co-founded the Resilient Machine Learning Institute, in collaboration with the École de Technologie Supérieure (Montreal), to enhance the resilience of critical communications systems with distributed AI/ML techniques. He is currently the Inventor of nine patents in wireless communications and the author of multiple IEEE publications.

FRANÇOIS GAGNON (Senior Member, IEEE) received the B.Eng. and Ph.D. degrees in electrical engineering from the École Polytechnique de Montréal.

He has been a Professor with the Department of Electrical Engineering, École de Technologie Supérieure (ÉTS), since 1991, where he has served as the Director, from 1999 to 2001, and has been holding the industrial research chair position, since 2001. In addition to holding the Richard J. Marceau Industrial Research Chair for the wireless Internet in developing countries, he is currently the NSERC-Ultra Electronics Chair in wireless emergency and tactical communication, the most prestigious industrial chair program in Canada. He also founded the Communications and Microelectronic Integration Laboratory and was its first Director. He has been very involved in the creation of the new generation of high-capacity line-of-sight military radios offered by Ultra Electronics Tactical Communication Systems (TCS). Ultra Electronics TCS and ÉTS have obtained the NSERC Synergy Prize for this collaboration. He is also actively involved in the SmartLand project of UTPL, Ecuador, the STARACOM strategic research networks, and the Réseau Québec Maritime. He serves on the boards of funding agencies and companies. Most recently, he was appointed as the Director General of ÉTS, in June 2019. His research interests include wireless communications, modulation, coding, microelectronics, signal processing, equalization, software-defined radio, mobile communication, and fading channels.